PHYSICAL REVIEW B VOLUME 16, NUMBER 1 1 JULY 1977

Lattice dynamics of wustite (FeO)

G. Kugel and C. Carabatos
Laboratoire de Physique des Milieux Condensés, Faculté de Sciences, Metz, France

B. Hennion
Centre d'Etudes Nucléaires de Saclay, Bôite Postale 2, 91190 Gif-sur-Yvette, France

B. Prevot
Laboratoire de Spectroscopie, Institut de Physique, Université L. Pasteur, Strasbourg, France

A. Revcolevschi
Laboratoire de Chimie Appliquée de l'Etat Solide, Centre National de la Recherche Scientifique, Vitry sur Seine, France

D. Tocchetti
Institut Laue-Langevin, Grenoble, France

(Received 15 December 1976)

Phonon dispersion curves of wustite (FeO) have been measured at room temperature by inelastic neutron scattering in the three high-symmetry directions [001], [110], and [111] of reciprocal space. The experimental curves are interpreted by various lattice-dynamical models including rigid-ion and shell models. The models show that both ions are highly polarizable and that overlap effects seem to play an important role on the shell charge Y_1 of the iron ion, and on the second-neighbor interaction constants. The best-fit model has been applied in calculating structure factors, optical and elastic constants, and the frequency-distribution function.

I. INTRODUCTION

FeO is one of the antiferromagnetic oxides having the NaCl structure in the paramagnetic phase.[1,2] In this class of transition-metal monoxides, dynamical properties are of great interest for theoretical and experimental reasons. The antiferromagnetic ordering below the Néel temperature is accompanied by a weak distortion, lowering the symmetry. FeO becomes rhombohedral under $T_N = 198$ °K, with a weak (1%) elongation along the [111] axis. The antiferromagnetic structure is of type II[1,2] (see Fig. 1). The moments of the (111) ferromagnetic planes reverse from one plane to the other. The magnetic moments point in the [111] direction.

The ground state of Fe^{2+} ion is a triplet state.[1] The splitting by the cubic and the rhombohedral crystal field is at the origin of a nonquenched orbital angular momentum. Therefore, lattice and spin dynamics have to be investigated intensively to see how the 3*d* metal electrons act on the force constants and on magnetic properties such as exchange interaction, magnetic anisotropy, magnetostriction, and elasticity. Spin-orbit coupling plays an important role in phonon-magnon interaction, which may occur in this compound.

The aim of the present investigation of FeO is to contribute to a better understanding of the lattice dynamics. So far, phonon measurements were reported for CoO,[3] MnO,[4,5] and NiO.[6] There is good agreement between theoretical and experimental results in the case of NiO and MnO, but a large ambiguity remains in the acoustic branches of CoO, which can be affected by the existence of magnetic excitations.

In Sec. II, experimental details are given together with the results, which are analyzed in

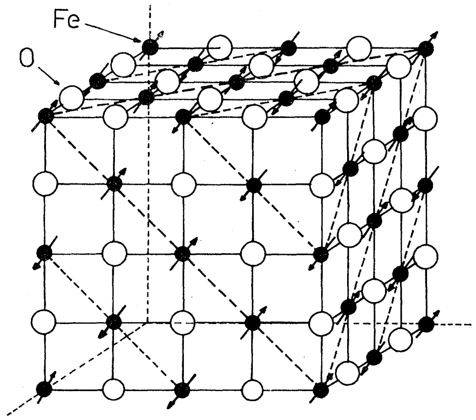

FIG. 1. Crystalline and antiferromagnetic structure of FeO below Néel temperature. Magnetic moments are arrayed in ferromagnetic sheets parallel to (111) planes (dashed line). The moment direction is perpendicular to the (111) sheets and points alternatively up and down in adjacent sheets.

Sec. III with the help of rigid-ion and shell models. In Sec. IV, we discuss our interpretation and give some related physical quantities calculated from our best-fit model.

II. EXPERIMENT AND RESULTS

A. Sample preparation

Single-crystalline iron protoxide was prepared by a floating-zone technique using an image furnace.[7] Powder mixtures of good-purity (99.99%) iron and iron sesquioxide Fe_2O_3 corresponding to a $Fe_{0.93}O$ stoichiometry of the protoxide were pressed isostatically into $0.8\times0.8\times8.0$ cm parallelepipeds. These were placed on platinum foils in alumina boats and sintered in an argon gas flow at 1100 °C for 15 h. The rods were rapidly cooled at room temperature by quick removal (still under argon) of the alumina boats from the hot zone of the sintering furnace. Such a procedure avoids partial decomposition of the resulting protoxide into magnetite and iron.

The crystal growth was carried out in a device described in detail elsewhere.[8] A liquid vertical zone was established between a sintered feed rod and a ⟨100⟩ oriented seed. The liquid zone was gradually moved along the sintered rod at a rate of about 1.5 cm/h, yielding a crystal. The operation was carried out under a flow of argon. The high-temperature gradient associated with image furnace heating introduced a good enough quenching to avoid decomposition of the crystal.

The samples obtained by this technique were black cylinders, a few centimeters long, from which it was possible to cut a single crystal having a volume of about 1 cm^3. Neutron elastic Bragg scattering shows the existence of a [100] axis nearly along the cylinder axis, as well as some imperfections.

B. Inelastic neutron scattering

The phonon-dispersion curves were measured by using triple-axis spectrometers, the crystal being oriented with [001] and [110] axes vertical, which allowed us to measure the three high-symmetry directions [001], [110], and [111]. The acoustic branches, with energies up to 8 THz, were determined on the triple-axis spectrometer H4 at the EL3 reactor of Centre d'Etudes Nucléaires, Saclay. The monochromator and analyzer were, respectively, germanium and pyrolytic graphite crystals. The optical and some acoustical branches were measured on the triple-axis spectrometer IN1 at the hot source of HFR of the Institut Laue-Langevin, Grenoble. In this case, Cu(200) and pyrolytic graphite (002) were used as monochromator and analyzer, respectively. The measurements were done at room temperature; the sample being paramagnetic, no magnetic ordering may disturb the experiments.

The measurement zones were determined by focusing[9] and structure-factor preliminary calculations. Some typical experimental neutron groups are represented in Fig. 2. The energy and momentum transfer due to the phonon is determined with an acceptable error by comparing an experimental group and a corresponding theoretical group. The calculation of this theoretical group consists in a convolution of the resolution function of the spectrometer[9,10] and the cross section of inelastic scattering, in which the dispersion law must be defined through parameters such as position, gradient, and curvature. The dispersion law is chosen so that correct adjustment between experimental and theoretical group is obtained.

Figure 3 represents a typical case applied to a longitudinal-acoustic phonon. Table I gives the measured phonons in THz units. The experimental dispersion curves in the three symmetry directions are given in Figs. 4 and 5.

The frequencies of the transverse- and longitudinal-optic modes at the center of the Brillouin zone are in good agreement with the infrared reflectivity results of Meftah *et al.*[11]

III. MODELS

In materials such as transition-metal monoxides, the interatomic forces are divided into two types, long-range or Coulomb electrostatic forces and short-range forces due to covalency and interatomic repulsion due to overlapping effects,[12-14] for example.

The long-range interactions are calculated with the help of the well known Ewald method.[15,16] The short-range forces are described in terms of parameters using the technique developed by Born and Von Karman.[14,17,18]

In the face-centered-cubic NaCl structure, the most general tensorial harmonic forces between first and second neighbors are described by means of eight parameters: two parameters A_{12} and B_{12}, the radial and tangential components of the axially symmetric force between first-neighbor ions, six parameters A_{ii}, B_{ii}, and D_{ii} (with $i=1$ for iron, $i=2$ for oxygen), for the radial and tangential components of the axially dissymmetric second-neighbor forces.[19] These eight parameters and an effective charge Z (Ref. 20) determined entirely a rigid-ion model with short-range forces extending to second neighbors.

In the general case of the dipole-approximation model or shell model of Dick and Overhauser[21] and

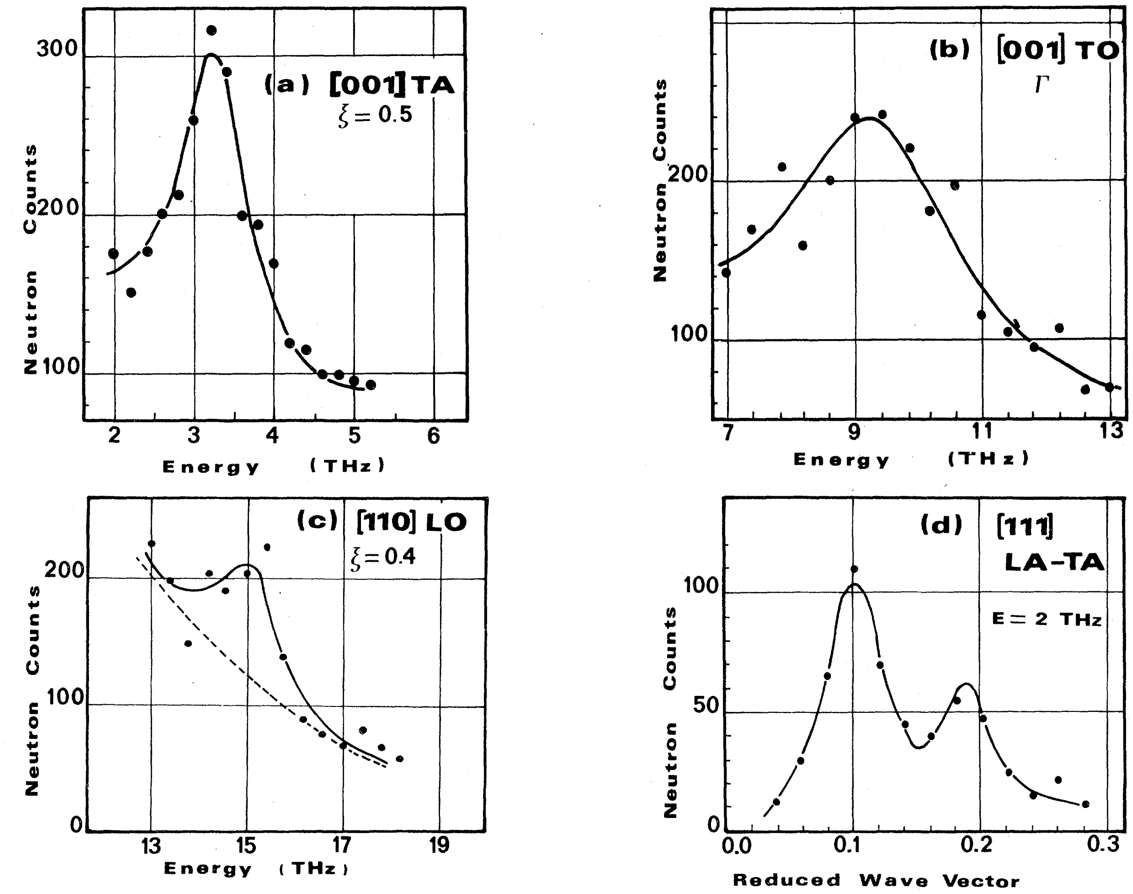

FIG. 2. Selected phonon groups in FeO. Group (a) is a transverse-acoustic mode along the [001] direction at $q = 0.5q_{\max}$. Group (b) is a transverse-optic mode at the zone center. Group (c) is a longitudinal-optic mode along the [111] direction at $q = 0.4q_{\max}$. Group (d) are acoustic modes along the [111] direction with a frequency of 2 THz.

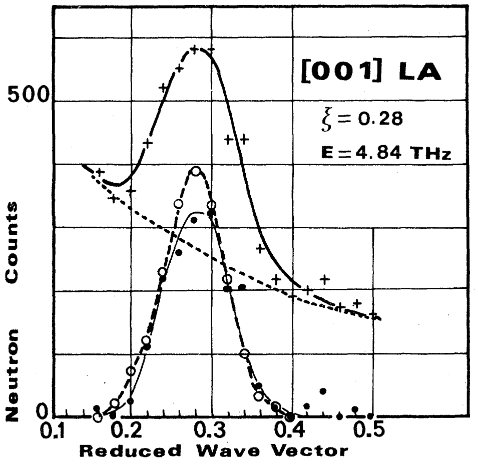

FIG. 3. Resolution of an experimental neutron group. Crossed points and heavy lines correspond to the experimental group, full points and thin line to experimental group without estimated background noise. Circles and heavy dashed line represent the theoretical group calculated by means of the resolution function of the three axes.

Cowley *et al.*,[18] the forces include shell-shell interaction S, core-shell interaction T, and core-core interaction R. The dynamical matrix becomes then

$$\underline{D} = \underline{M}^{-1/2}[(\underline{R} + \underline{Z}\underline{C}\underline{Z}) - (\underline{T} + \underline{Z}\underline{C}\underline{Y})$$
$$\times (\underline{S} + \underline{Y}\underline{C}\underline{Y})^{-1}(\underline{T} + \underline{Y}\underline{C}\underline{Z})]\underline{M}^{-1/2},$$

where the elements of the 6×6 $\underline{R}$, $\underline{T}$, and $\underline{S}$ matrices are the Fourier transforms of the force constants of the same name; $\underline{M}$ is the mass matrix.

We have used the approximations due to Cowley and Cochran[13,18]; thus, our most general model is then specified by 17 parameters: A_{12}, B_{12}, A_{11}, B_{11}, D_{11}, A_{22}, B_{22}, D_{22}, α_1, α_2, d_1, d_2, $\beta_t(12)$, $\beta_t(21)$, α_S, β_S, and Z.[22]

For the shell model, α_1 and α_2 are the individual electronic polarizabilities with no interference factor.

We obtained the best values of the model parameters by means of the nonlinear least-squares-fitting program of Marquardt.[23] The results of

TABLE I. Phonon frequencies in THz units in FeO at room temperature along the three high-symmetry directions.

	$\xi = q\frac{2\Pi}{a}$	TA	LA	TO	LO	
Γ	0.0	0.0	0.0	9.6 ± 0.4	15.8 ± 0.4	
	0.14 ± 0.01		2.42			
	0.2			9.7 ± 0.3	15.5 ± 0.6	
	0.23 ± 0.02		3.63			
	0.28 ± 0.02		4.68			
	0.34 ± 0.02	2.42				
	0.38 ± 0.02		6.05			
Δ	0.4			9.9 ± 0.3	14.4 ± 0.4	
	0.5	3.3 ± 0.15	6.6 ± 0.2			
	0.6		7.1 ± 0.2	10.4 ± 0.4	14.0 ± 0.4	
	0.7	4.0 ± 0.15				
	0.8		6.6 ± 0.2	10.5 ± 0.4	13.6 ± 0.3	
	0.85	4.4 ± 0.2				
X	1.0	4.4 ± 0.15	6.3 ± 0.3	11.1 ± 0.4	13.8 ± 0.4	
	$\xi = q\sqrt{2}\frac{2\Pi}{a}$	TA 1	TA 2	LA	TO	LO
Γ	0.0	0.0	0.0	0.0	9.6 ± 0.4	15.8 ± 0.4
	0.095 ± 0.005			2.45		
	0.15 ± 0.015			3.63		
	0.2				10.3 ± 0.4	15.6 ± 0.4
	0.22 ± 0.015			4.84		
	0.24 ± 0.015	2.42				
	0.29 ± 0.015		3.0			
	0.3	2.8 ± 0.15		6.0 ± 0.15		
Σ	0.35	3.4 ± 0.2				
	0.32 ± 0.02			7.2 ± 0.2		
	0.4	3.8 ± 0.2			10.4 ± 0.4	15.2 ± 0.3
	0.5			7.5 ± 0.25		
	0.6	4.6 ± 0.2	5.10 ± 0.15		12.2 ± 0.4	14.6 ± 0.5
	0.8	4.6 ± 0.3			13.2 ± 0.4	12.2 ± 0.4
	0.82 ± 0.02			6.0		
X	1.0	4.4 ± 0.15	6.3 ± 0.15	4.3 ± 0.15	13.8 ± 0.4	11.1 ± 0.4
	$\xi = q\frac{2\Pi}{a}\sqrt{3}$	TA	LA	TO	LO	
Γ	0.0	0.0	0.0	9.6 ± 0.4	15.8 ± 0.4	
	0.08 ± 0.005		2.0			
	0.17 ± 0.001	2.0	3.8 ± 0.2			
Λ	0.2		5.8 ± 0.2	9.2 ± 0.4	15.2 ± 0.4	
	0.25 ± 0.02	3.0 ± 0.15				
	0.4	4.0 ± 0.2		8.6 ± 0.4	15.2 ± 0.4	
L	0.5		8.3 ± 0.3			

these calculations are shown in Table II, where five versions of the model with the $\underline{R} = \underline{T} = \underline{S}$ assumption for the shell model are presented. Model I is a rigid-ion model with first- and second-neighbor interactions limited to oxygen-oxygen interactions. Model II is a rigid-ion model with first- and second-neighbor interactions limited to iron-iron interactions. Model III is a complete rigid-ion model with effective charge Z'. Model IV is a shell model with first neighbor interaction and both ions polarizable. Model V is the same shell model with first- and second-neighbor interactions.

With the 17-parameter model, the fitting is hardly better, in spite of the great number of parameters. We thus consider that model V is the best model from the statistical point of view.

The standard error σ and the χ^2 test given in Table II are calculated by application of the following relations:

$$\sigma = \left(\sum_{i=1}^{N} \frac{(\omega_{\text{obs}}^{i} - \omega_{\text{mod}}^{i})^2}{N-K} \right)^{1/2},$$

$$\chi^2 = \frac{1}{N-K} \sum_{i=1}^{N} \left(\frac{\omega_{\text{obs}}^{i} - \omega_{\text{mod}}^{i}}{\Delta\omega_i} \right)^2,$$

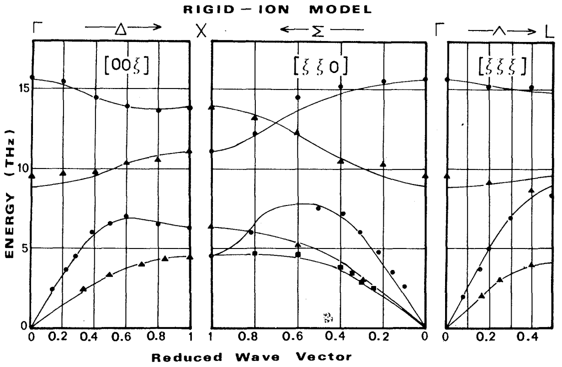

FIG. 4. Phonon-dispersion curves in FeO by inelastic neutron scattering at room temperature. The experimental points are represented by ●, ▲, and ■ for, respectively, longitudinal, transverse 1 and 2 modes. The measurements are compared with the least-square-fitting rigid-ion model III.

where N is the number of observed phonons, K is the number of adjustable parameters, ω_{obs} is the measured phonon frequency, ω_{mod} the model frequency, and $\Delta\omega$ the estimated experimental error.

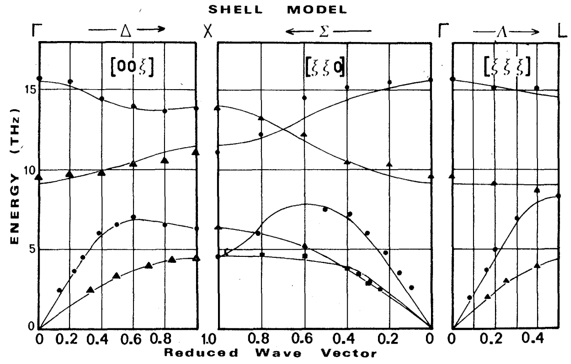

FIG. 5. Phonon dispersion curves in FeO and shell-model V.

The theoretical dispersion curves of models III and V are represented in Figs. 4 and 5.

IV. DISCUSSION–CALCULATIONS FROM MODELS

Some preliminary remarks may be made before discussing some specific aspects of the models; at first, the second-neighbor force constants in

TABLE II. Model parameters for the best-fitting models in FeO. These parameters were obtained by least-squares fitting. They are defined as in Ref. 19. Indices 1 and 2 refer, respectively, to iron and oxygen. Models I, II, and III are rigid-ion models; IV and V are shell models. (e stands for electron charge; v stands for volume of the unit cell.)

		Models				
Model parameter	Units	Rigid ion I	Rigid ion II	Rigid ion III	Shell model IV	Shell model V
Short range						
A_{12}	e^2/v	12.843	15.324	14.364	23.579	36.054
B_{12}	e^2/v	−1.211	−2.502	−2.441	−3.90	−6.737
A_{11}	e^2/v	0.0	2.264	1.955	0.0	−3.389
B_{11}	e^2/v	0.0	−2.158	−1.629	0.0	−0.918
D_{11}	e^2/v	0.0	1.882	1.243	0.0	1.768
A_{22}	e^2/v	2.821	0.0	0.871	0.0	−0.924
B_{22}	e^2/v	−1.54	0.0	0.013	0.0	0.702
D_{22}	e^2/v	0.397	0.0	0.156	0.0	−0.417
T interaction						
$\beta_T(12)$	···	1.0	1.0	1.0	1.0	1.0
$\beta_T(21)$	···	1.0	1.0	1.0	1.0	1.0
Polarizabilities						
α_1	$1/v$	···	···	···	0.052	0.075
α_2	$1/v$	···	···	···	0.064	0.10
d_1	e	···	···	···	−0.333	−0.484
d_2	e	···	···	···	0.359	0.858
Ionic charge						
Z	e	0.967	0.997	0.956	1.587	2.0
S interaction						
α_S	···	1.0	1.0	1.0	1.0	1.0
β_S	···	1.0	1.0	1.0	1.0	1.0
Standard error σ	THz	0.72	0.44	0.36	0.46	0.33
Fitting error χ^2	···	3.6	1.58	0.96	1.42	0.90

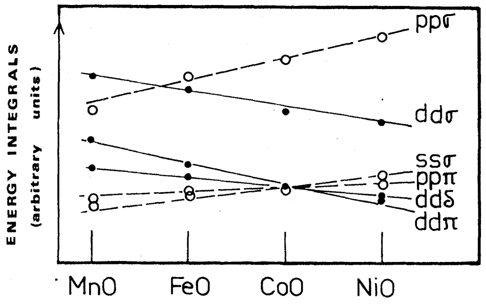

FIG. 6. Slater-Koster energy integrals for the MnO, FeO, CoO, NiO series. The variation of Slater-Koster energy integrals of the series between second neighbors, calculated by Mattheiss are represented. Metal-metal interactions are in full points, oxygen-oxygen ones in circles. Type of orbitals involved are given at the right side.

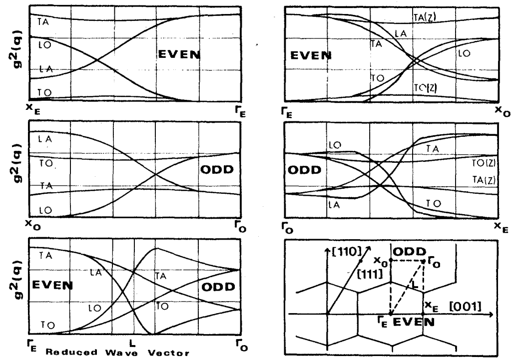

FIG. 7. Reduced structure factor in FeO. Inelastic reduced structure factor for FeO is calculated on the basis of a simple shell model and is plotted in arbitrary units. Calculation paths are represented on the lower right diagram. TA(z) and TO(z) are modes propagating along [110] direction and polarized along [001].

the range of 15% of the first-neighbor ones cannot be neglected. Both ions are highly polarizable. The assumption $R = T = S$ is satisfactory.

The negative sign of the mechanical polarizability d_1 of the metallic ion is at first sight surprising. The parameter d_1 is related to the shell charge Y_1 by

$$d_1 = \frac{-Y_1 R_0}{R_0 + k_1} \quad \text{with} \quad R_0 = \frac{e^2}{V}(A_{12} + 2B_{12}) .$$

The negative sign of d_1 implies a positive sign of the shell charge Y_1 of the iron ion. Cowley[18] explained this sign by the creation of dipoles in the region where the overlapping between electronic clouds of iron and oxygen is maximum. Furthermore, Bilz *et al.*[24] has interpreted the positive sign Y_1 by considering excited states in the overlap region,[25] where the total charge density is smaller than the exact superposition of the two charge densities of the individual ions. This produces a redistribution of charges—in other words, a "pseudodeformability," the total effect being described by positive overlap charges located on the metallic ions.

If we consider second-neighbor interactions, we see, in Table II, that iron-iron force constants are, in absolute value, greater than oxygen-oxygen ones in spite of the ionic radii. Keeping in mind that short-range interactions have their origin mainly in overlapping effects,[26] it is possible to compare the first- and the second-neighbor interaction parameters with Slater-Koster energy integrals[27] calculated by Mattheiss[28] in band-structure calculations of the whole series MnO, CoO, FeO, and NiO. (See Fig. 6.)

This comparison implies the following remarks:

TABLE III. Optical and elastic constants in FeO. Infrared results are from Ref. 11. Neutron elastic constants are calculated from the dispersion curve slopes near the center of the Brillouin zone.

Constants	Units	Infrared	Neutrons	Model III	Model V
ω_{LO}	THz	16.05	15.8	15.8	15.8
	cm^{-1}	535	526	526	526
ω_{TO}	THz	8.7	9.6	9.1	8.85
	cm^{-1}	290	320	303	295
ϵ_0	⋯	32.8	⋯	3.01	31.4
ϵ_∞	⋯	9.63	⋯	1.0	9.24
C_{11}	10^{12} dyn/cm^2	⋯	3.59	2.94	3.02
C_{12}	10^{12} dyn/cm^2	⋯	1.56	1.39	1.21
C_{44}	10^{12} dyn/cm^2	⋯	0.563	0.52	0.70

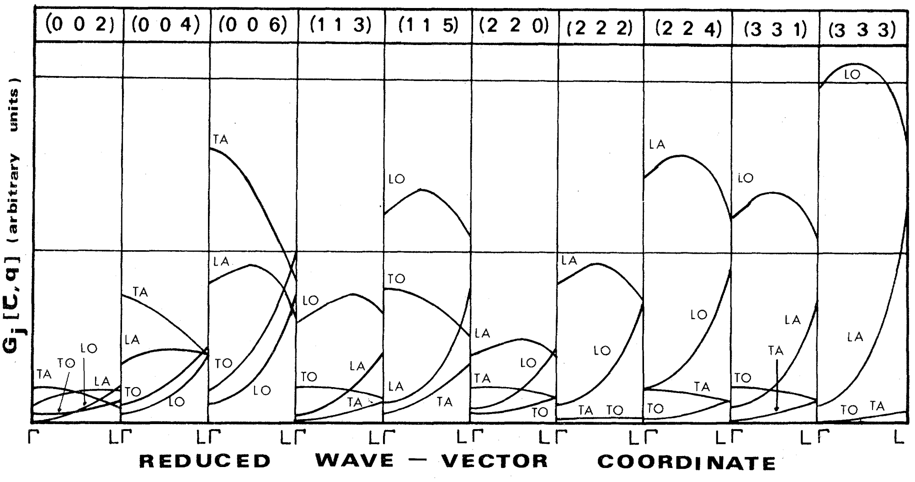

FIG. 8. Total structure factor in FeO in the [111] direction. Inelastic total structure factor for FeO is calculated on the basis of model V. Calculation is made in several Brillouin zones. The diagram gives the factor in the [111] direction with arbitrary units.

the first-neighbor force constants of several models[3-5,29] do not differ appreciably (20%), as neither do the Slater-Koster corresponding energies of band-structure calculation. There is a similarity in the variation of the Slater-Koster energies of second neighbors and corresponding force constants (Fig. 6). This correspondance has to be verified more accurately by applying the same model to the different *M*O series (*M* stands for metal). If our remark is confirmed, it may reveal an interesting feature for the case of 3*d* electrons.

Our calculation considers only dipole deformations (of symmetry T_{1u} in cubic structure). Monopole deformation given by the breathing shell model[30] and quadrupolar deformation (E_g symmetry) have not been applied. The decreasing of the transverse-optic branch in the [111] direction and the small value of C_{44} (Table III) may be an effect of quadrupolar interactions.[31-33]

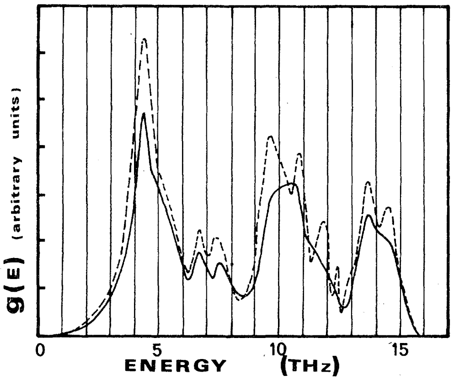

FIG. 9. Density of phonon states in FeO at room temperature. The results of Gilat's program calculation is given with two different channel widths.

Keeping in mind the above remarks, we calculate the general and reduced form[17,34] of the dynamical structure factor of FeO (Figs. 7 and 8), as well as the frequency-distribution function[35] represented in Fig. 9. Elastic constants, high-frequency dielectric constants, and small-q-value optical frequencies for the two models III and V were also calculated. In Table III, the optical values are compared to results of infrared measurements.[11] The agreement between optic modes is good.

V. CONCLUSION

We have presented measurements of phonon frequencies along the high-symmetry directions in FeO at room temperature. The frequencies experimentally found agree quite well with a shell-model calculation. Nevertheless, quadrupolar deformation of electronic clouds probably have to be considered to get better agreement. Two interesting aspects have been pointed out: The shell charge of the iron ion is positive; the relative values of second-neighbor interactions vary with respect to band-structure results.

ACKNOWLEDGMENTS

We would like to thank Professor M. Sieskind for his interest in the present work and for stimulating propositions and discussions. We are grateful to Professor H. Bilz and to Dr. B. Dorner for many fruitful discussions. We are indebted to Dr. G. Dhalenne for experimental help in crystal preparation. We would like to thank Dr. W. Kress for helpful discussions.

[1] J. Kanamori, Prog. Theor. Phys. 17, 177 (1957).

[2] C. G. Shull, W. A. Strauser, and E. O. Wollan, Phys. Rev. 83, 333 (1951).

[3] J. Sakurai, W. J. L. Buyers, R. A. Cowley, and G. Dolling, Phys. Rev. 167, 510 (1968).

[4] B. C. Haywood and M. F. Collins, J. Phys. C 4, 1299 (1971).

[5] V. Wagner, W. Reichardt, and W. Kress (unpublished).

[6] W. Reichardt, V. Wagner, and W. Kress, J. Phys. C 8, 3955 (1975).

[7] M. Saurat and A. Revcolevschi, Rev. Hautes Temp. Refract. 8, 291 (1971).

[8] A. Revcolevschi, Rev. Hautes. Temp. Refract. 7, 73 (1960).

[9] M. J. Cooper and R. Nathans, Acta. Crystallogr. 23, 357 (1967).

[10] B. Dorner, Acta. Crystallogr. A 28, 319 (1972).

[11] M. Meftah, B. Prevot, and M. Sieskind (unpublished).

[12] G. K. Horton and A. A. Maradudin, *Dynamical Properties of Solids* (North-Holland, Amsterdam, 1974), Vol. 1.

[13] W. Cochran, Crit. Rev. Solid State Sci. 2, (1971).

[14] M. Born and K. Huang, *Dynamical Theory of Crystal Lattices* (Oxford U. P., Oxford, 1954).

[15] P. P. Ewald, Ann. Phys. Leipz. 64, 253 (1921).

[16] E. W. Kellermann, Phil. Trans. R. Soc. Lond. A 238, 513 (1940).

[17] A. D. B. Woods, W. Cochran, and B. N. Brockhouse, Phys. Rev. 119, 980 (1960).

[18] R. A. Cowley, W. Cochran, B. N. Brockhouse, and A. D. B. Woods, Phys. Rev. 131, 1030 (1963).

[19] M. J. L. Sangster, G. Peckham, and D. H. Saunderson, J. Phys. C 3, 1026 (1970).

[20] B. Szigetti, Proc. R. Soc. A 204, 51 (1950).

[21] B. G. Dick and A. W. Overhauser, Phys. Rev. 112, 90 (1958).

[22] C. Carabatos, B. Hennion, K. Kunc, F. Moussa, and C. Schwab, Phys. Rev. Lett. 26, 770 (1971).

[23] D. W. Marquardt, J. Soc. Ind. Appl. Math. 11, 431 (1963).

[24] H. Bilz, M. Buchanan, K. Fischer, and R. Haberkorn, Solid State Commun. 16, 1023 (1975).

[25] R. Zeyher, Phys. Status Solidi B 48, 711 (1971).

[26] H. Bilz, B. Gliss, and W. Hanke, *Dynamical Properties of Solids*, edited by G. K. Horton and A. A. Maradudin (North-Holland, Amsterdam, 1974), Vol. 1,

[27] J. C. Slater and G. F. Koster, Phys. Rev. 94, 1498 (1954).

[28] L. F. Mattheiss, Phys. Rev. B 5, 290 (1972).

[29] T. P. Sharma, Solid State Commun. 15, 1171 (1974).

[30] U. Schroeder, Solid State Commun. 4, 347 (1966).

[31] W. Bluthardt, W. Schneider, and M. Wagner, Phys. Status Solidi B 56, 453 (1973).

[32] K. Fischer, H. Bilz, R. Haberkorn, and W. Weber, Phys. Status Solidi B 54, 285 (1972).

[33] K. Fischer, Phys. Status Solidi B 66, 295 (1954).

[34] W. Marshall and S. W. Lovesey, *Theory of Thermal Neutron Scattering* (Clarendon, Oxford, 1971).

[35] G. Gilat and L. J. Raubenheimer, Phys. Rev. 144, 390 (1966).